

PARTICLE ACCELERATION IN AN EVOLVING NETWORK OF UNSTABLE CURRENT SHEETS

LOUKAS VLAHOS, HEINZ ISLIKER, AND FABIO LEPRETI

Department of Physics, University of Thessaloniki, Thessaloniki 54 124, Greece

Received 2003 November 20; accepted 2004 February 20

ABSTRACT

We study the acceleration of electrons and protons interacting with localized, multiple, small-scale dissipation regions inside an evolving, turbulent active region. The dissipation regions are unstable current sheets (UCSs), and in their ensemble they form a complex, fractal, evolving network of acceleration centers. Acceleration and energy dissipation are thus assumed to be fragmented. A large-scale magnetic topology provides the connectivity between the UCSs and in this way determines the degree of possible multiple acceleration. The particles travel along the magnetic field freely without losing or gaining energy until they reach a UCS. In a UCS, a variety of acceleration mechanisms are active, with the end result that the particles depart with a new momentum. The stochastic acceleration process is represented in the form of continuous-time random walk, which allows one to estimate the evolution of the energy distribution of the particles. It is found that under certain conditions, electrons are heated and accelerated to energies above 1 MeV in much less than 1 s. Hard X-ray and microwave spectra are calculated from the electrons' energy distributions, and they are found to be compatible with the observations. Ions (protons) are also heated and accelerated, reaching energies up to 10 MeV almost simultaneously with the electrons. The diffusion of the particles inside the active region is extremely fast (anomalous superdiffusion). Although our approach does not provide insight into the details of the specific acceleration mechanisms involved, its benefits are that it relates acceleration to the energy release, it well describes the stochastic nature of the acceleration process, and it can incorporate the flaring large-scale magnetic topology, potentially even its temporal evolution.

Subject headings: acceleration of particles — Sun: flares — Sun: particle emission

1. INTRODUCTION

Solar flares remain, after almost 100 years of intense study, an unsolved problem for astrophysics. We define as “flare” the sporadic transformation of magnetic energy to (1) plasma heating, (2) particle acceleration, and (3) plasma flows. It seems that the total magnetic energy released in a single flare is not spread equally to all three components. The energetic particles carry a very large fraction of the total energy released during a flare, reaching sometimes up to 50% (Saint-Hilaire & Benz 2002).

Modeling the explosive energy release requires methods that can simultaneously treat the large-scale magnetic field structures and the small-scale dissipation events. The convection zone actively participates in the formation and evolution of large-scale structures by rearranging the position of the field lines and at the same time adds new magnetic flux (emerging flux) and new stresses to the existing topologies. The loss of stability of several looplike structures forms large-scale disturbances (coronal mass ejection), which further disturb the preexisting and thus far stable large-scale structures. In this way, the three-dimensional magnetic topologies are constantly forced away from the potential state (if they ever reach one) because of slow or abrupt changes in the convection zone. All these nonpotential magnetic stresses force the large-scale magnetic topology to form short-lived, small-scale magnetic discontinuities in order to dissipate the excess energy in localized current sheets. This conjecture was initially proposed by Parker (1988), and it was subsequently modeled using three-dimensional MHD numerical simulations by many researchers (see, e.g., the work of Nordlund & Galsgaard 1996). *We emphasize here that the concept of sudden formation of a distribution of unstable discontinuities inside a well-organized*

large-scale topology has not been appreciated or used extensively enough to model the solar flare phenomenon.

The scenario of spatially distributed, localized, small-scale dissipation, which moreover evolves in time, is supported by observations that indicate highly fragmented energy dissipation and particle acceleration processes. There is strong evidence that narrowband millisecond spike emission in the radio range is directly associated with the primary energy release events. The emission itself of the radio spikes is fragmented in space and time, as is seen in radio spectrograms and in spatially resolved observations. It must thus be concluded that the energy release process is also fragmented in space and time, to at least the same degree as the radio spike emission (see Benz 2003). Also, type III burst radio emission caused by electron beams escaping from flaring regions exhibits fragmentation as a strong characteristic (e.g., Benz 1994). It is too simple an interpretation of the available data that the large-scale structures seen have a relatively simple topology down to all scales.

One approach that is capable of capturing the full extent of this interplay of highly localized dissipation in a well-behaved large-scale topology (“sporadic flaring”) is based on a special class of models that use the concept of self-organized criticality (SOC; Bak et al. 1987). The main idea is that active regions evolve by the continuous addition of new or the change of existing magnetic flux on an existing large-scale magnetic topology, until at some point(s) inside the structure magnetic discontinuities are formed and the currents associated with them reach a threshold. This causes a fast rearrangement of the local magnetic topology and the release of the excess magnetic energy at the unstable point(s). This rearrangement may in turn cause the lack of stability in the neighborhood, and so forth, leading to the appearance of flares (avalanches) of all sizes that follow a well-defined statistical

law (Lu & Hamilton 1991; Lu et al. 1993; Vlahos et al. 1995; Isliker et al. 2000, 2001), which agrees remarkably well with the observed flare statistics (Crosby et al. 1993).

The solar atmosphere cannot be modeled exclusively with the use of high-resolution MHD numerical codes. The small-scale discontinuities easily give rise to kinetic instabilities and anomalous resistivity, which play a very important role; they dramatically change the evolution of even the large-scale structures. On the other hand, numerical codes following the evolution of charged particles in idealized, nonevolving, large-scale current sheets also fail to capture the spatio-temporal evolution of the magnetic energy dissipation. The extraordinary efficiency of particle acceleration during solar flares questions the use of ideal MHD for the description of flares, since it misses kinetic plasma effects, which yet play a major role in the energy dissipation process and for the local state of the plasma. The coupling of the large scale and the small scale is extremely difficult to handle, not only in solar physics but in physics in general, and it is the main reason for not having resolved the solar flare problem for so many years (Cargill 2002).

Our inability to properly describe the coupling between the MHD evolution and the kinetic plasma aspects of the driven flaring region is the main reason behind our lack of understanding of the mechanism(s) that causes the acceleration of high-energy particles. Let us now define more accurately the so-called acceleration problem. *We need to understand the mechanism(s) that accelerate electrons and ions in relatively large numbers to energies well above the relativistic regime on a short timescale with specific energy spectra for the different isotopes and charge states.*

Let us summarize very briefly the main observational constraints for the acceleration processes in solar flares.

Electrons.—Electron energies well in excess to 100 keV, and occasionally up to tens of MeV, are inferred. Electrons reach 100 keV in less than 1 s and higher energies in a few seconds. The number of electrons required above 20 keV is large for X-class flares and can reach up to 10^{38} electrons s^{-1} , although this number is model-dependent and not very accurate (see, e.g., Miller et al. 1997). The observed spectra in the hard X-rays (HXR) can be fitted with single or double power laws, combined often—but not always—with a thermal emission spectrum at the lowest energies (Holman 2003; Holman et al. 2003; Piana et al. 2003). The spectra in the microwaves roughly show a power-law decay at high frequencies (Holman 2003).

Ions.—Ions (especially protons) are inferred to have energies above 1 MeV and up to 1 GeV per nucleon. The 10 MeV ions are accelerated on the same timescales as the electrons, with the high-energy ions delayed up to 10 s. The total number of ions accelerated may carry the same energy as the electrons. The continuous component of the γ -ray spectra are usually power laws. An important finding is the massive enhancement of ${}^3_2\text{He}$ in very impulsive flares (see, e.g., Miller et al. 1997).

Acceleration mechanisms.—Numerous books and reviews have been devoted to the challenging problem of particle acceleration (Heyvaerts 1981; Vlahos et al. 1984; Melrose 1992; Vlahos 1994, 1996; Kirk 1994; Kuijpers 1996; Miller et al. 1997). The proposed models usually address parts of the problem, and almost all acceleration mechanisms have no clear connection to the large-scale topology and to the magnetic energy release mechanism(s). The most prominent mechanisms are shock waves (Holman & Pesses 1983; Blandford & Eichler 1987; Ellison & Ramaty 1985; Decker 1988), MHD turbulence (Fermi 1949; Miller & Roberts 1995), and DC

electric fields (Benka & Holman 1992; Moghaddam-Taaheri et al. 1985; Moghaddam-Taaheri & Goertz 1990).

Mixing acceleration mechanisms.—Several inquiries have been made in which different acceleration mechanisms had been mixed.

Decker & Vlahos (1986) analyzed the role of shock drift acceleration (SDA) when the shock is surrounded by a turbulent spectrum. The SDA is fast but not efficient, since the particles drifting along the shock surface's electric field quickly leave the shock. The presence of turbulence reinforces the acceleration process by providing a magnetic trap around the shock surface and forcing a particle to return many times to the shock surface. The particle leaves the shock surface, travels a distance s_i inside the turbulent magnetic field, returns back to the shock surface with velocity v_i , drifts a distance l_i along the shock electric field E_{sc} , changing its momentum by $\Delta p_i \sim E_{sc}(l_i/v_i)$, it escapes again, travels a distance s_{i+1} before returning back to the shock and drifting along the electric field, in other words, the acceleration cycle has begun again. The process repeats itself several times before the particle gains enough energy to escape from the turbulent trap around the shock surface. Let us note some very important characteristics of this acceleration:

1. The distances s_i traveled by the particle before returning back to the shock are only indirectly relevant to the acceleration; they basically delay the process and influence the overall timing, i.e., the “acceleration time,” another important parameter of the particle acceleration process.
2. The energy gain depends critically on the lengths l_i the particle drifts along the shock surface, albeit in a statistical sense, i.e., on the distribution of the l_i , $i = 1, 2, 3, \dots$
3. The times τ_i a particle spends on the shock surface are again crucial for the energy gain and also, together with the s_i , for the estimation of the acceleration time.
4. For the total acceleration problem, which concerns the energies reached and the times needed to reach them, all three variables, s_i , l_i , τ_i , are of equal importance.

Ambrosiano et al. (1988) discussed a similar problem, placing a current sheet in a region of Alfvénic turbulence. In addition, here the ability of the associated DC electric field to accelerate particles is enhanced by the presence of the MHD turbulence. The acceleration process is again of a cyclic nature, as in the case of turbulent SDA, and the process is again characterized by the three variables s_i , l_i , and τ_i . The turbulent current sheet has several avenues to enhance the acceleration efficiency, since the plasma inflow is dynamically driven and causes a variety of new and still unexplored phenomena. Arzner (2002) analyzed the mixture of stationary MHD turbulence with a DC electric field. The trapping of the particles inside the turbulent magnetic field causes a new “collision scale,” and, in some circumstances, acceleration becomes dependent on an alternative “Dreicer field,” in which particle collisions are replaced by collisions with magnetic irregularities. Also, the diffusive shock acceleration is actually of a mixed type, having as elements a shock and magnetic turbulence, although turbulence plays a more passive role of just scattering the particles. It seems that most acceleration mechanisms are more or less of a mixed type.

We conclude that the mixture of mechanisms enhances the acceleration efficiency and removes some of the drawbacks attached to the different isolated mechanisms. A second main conclusion we draw is that “cyclic processes,” e.g., through

trapping around the basic accelerators, are important elements—if not the presupposition—of efficient and fast acceleration in space plasmas.

Can the Unstable Current Sheets (UCSs) naturally provide the unification of all the above mechanisms?—UCSs are the regions in which magnetic energy is dissipated, and it is natural to ask if they can become the actual source of the energetic particles. According to the existing understanding of UCSs, several potential mechanisms for particle acceleration coexist at a UCS. Plasma flows driving turbulence, shock waves, and DC electric fields are expected to appear simultaneously inside and around a driven and evolving UCS. If the UCS is located in the middle of a turbulent magnetic topology, all these phenomena will be enhanced and the sporadic external forcing of the plasma inflow into the UCS will create bursts of sporadic acceleration. The scenario of a single UCS currently enjoys very large popularity (e.g., Litvinenko 2003; Fletcher & Martens 1998; Martens 1988), and the question is as follows: Can one single UCS be the answer to the acceleration problem?

We believe that this is impossible, since a single, isolated UCS must be enormously large ($10^9 \times 10^9 \times 10^5$ m), remain stationary for a long time, and continuously accelerate particles with extreme efficiency in order to provide the required numbers of accelerated particles and the observed acceleration times. From the Earth's magnetic tail, it is known that large UCSs break up quickly, creating a network of smaller scale UCSs, with a specific probability distribution $P(l)$ of their characteristic scales, a process that is just a manifestation of turbulence (Angelopoulos et al. 1999). The formation of a large-scale helmet above certain loops, driven by erupting filaments, cannot be excluded entirely and represents a special class of very energetic phenomena (Masuda et al. 1994). We believe, however, that such a current sheet breaks down on a very short timescale, and the formation of smaller scale current sheets will be unavoidable. Eventually, even in this very special case the acceleration probably takes place in an environment similar to the one discussed in this paper.

There is a second reason, based on a result on the statistics of flares, for questioning the idea of a single, large-scale UCS that is associated with just one, or at most, two loops, as in the scenario sometimes called the standard model (see, e.g., Shibata et al. 1995). Wheatland (2000) determined the frequency distributions in total emitted energy of flares occurring in the *same, individual* active region (number of flares per unit energy), and they find featureless power-law distributions extending over many decades. If a single UCS were the basic mechanism behind a flare, then the energy output must be expected to be related to the physical properties of the individual active region, e.g., to the linear dimensions of the active region and the associated UCS, so that it is at least difficult to imagine how a single-site reconnection model could be able to produce a featureless energy distribution that extends over many decades. Our attempt in this paper is to take advantage of the positive properties of isolated UCSs as accelerators but at the same time to assume that the dissipation happens at *multiple, small-scale* sites.

The three-dimensional magnetic topology, driven from the convection zone, dissipates energy in localized UCSs, which are spread inside the coronal active region, providing a natural fragmentation for the energy release and a multiple, distributed accelerator. In this way, the magnetic topology acts as a host for the UCS, and the spatio-temporal distribution of the latter defines the type of a flare, its intensity, the degree of

energization and acceleration of the particles, the acceleration timescales, etc. Evolving large-scale magnetic topologies provide a variety of opportunities for acceleration that is not restricted to flares but can also take place before or after a flare, being just the manifestation of a more relaxed, but still driven topology. Thus, depending on the level to which the magnetic topology is stressed, particles can be accelerated without a flare to happen, and even long-lived acceleration in nonflaring active regions must be expected to occur. Consequently, the starting point of the model introduced below is a driven three-dimensional magnetic topology, which defines a time-dependent spatial distribution of UCSs inside the active region. In this paper, we focus on the interaction of the UCS with particles. The details of the mechanisms involved in the acceleration of particles inside the UCS are not essential in a stochastic modeling approach.

Ideas related to the basic approach of this paper have been presented earlier (Anastasiadis & Vlahos 1991, 1994; Vlahos 1993; Anastasiadis et al. 1997) but they left many points open for future development, not being as general and complete approaches as the model we present here. In the approach we follow here, we make extensive use of new developments in the theory of SOC models for flares. Also taken into account are ideas from the theory of complex evolving networks (Albert & Barabasi 2002; Dorogovtsev & Mendest 2002), albeit adjusted to the context of plasma physics; the spatially distributed, localized UCSs can be viewed as a network whose “nodes” are the UCSs themselves and whose “edges” are the possible particle trajectories between the nodes (UCSs). The particles are moving around in this network, forced to follow the edges, and undergoing acceleration when they pass by a node (see also Fig. 2). The network is complex in that it has a nontrivial spatial structure, and it is evolving since the nodes (UCSs) are short-lived, as are the connectivity channels, which change continually during the evolution of a flare. This instantaneous connectivity of the UCS is an important parameter in our model, it determines to what degree multiple acceleration is imposed onto the system, which in turn influences the instantaneous level of energization and the acceleration timescale of the particles.

In this paper, we introduce a stochastic, multiple acceleration model for solar flare particle acceleration. We assume an ensemble of UCSs, distributed in space in such a way that it reflects a relatively simple large-scale topology in which turbulence at small scales is developing. Concretely, the UCSs in their ensemble form a fractal, as is the case in the SOC models (H. Isliker & L. Vlahos 2003, unpublished; McIntosh et al. 2002). Particles move erratically around and occasionally enter a UCS in which they undergo acceleration. The acceleration process is taken as a simple DC electric field mechanism. The basic approach of the model is a combined random walk in position- and momentum-space. The framework we introduce is such that potentially all multiple acceleration models can be formulated in this framework, as long as the acceleration takes place in spatially localized, disconnected, small-scale regions. Our main interest here is in the diffusion, acceleration, and heating of the electrons. We follow the evolution of the kinetic energy distribution in time and calculate from these distributions the HXR and microwave spectra, which can be compared to the observations. We also briefly investigate the case of ion heating and acceleration.

The basic elements of our model are presented in § 2. In § 3, we present some of our results, and in § 4 we discuss our findings and propose ways for continuing the exploration of

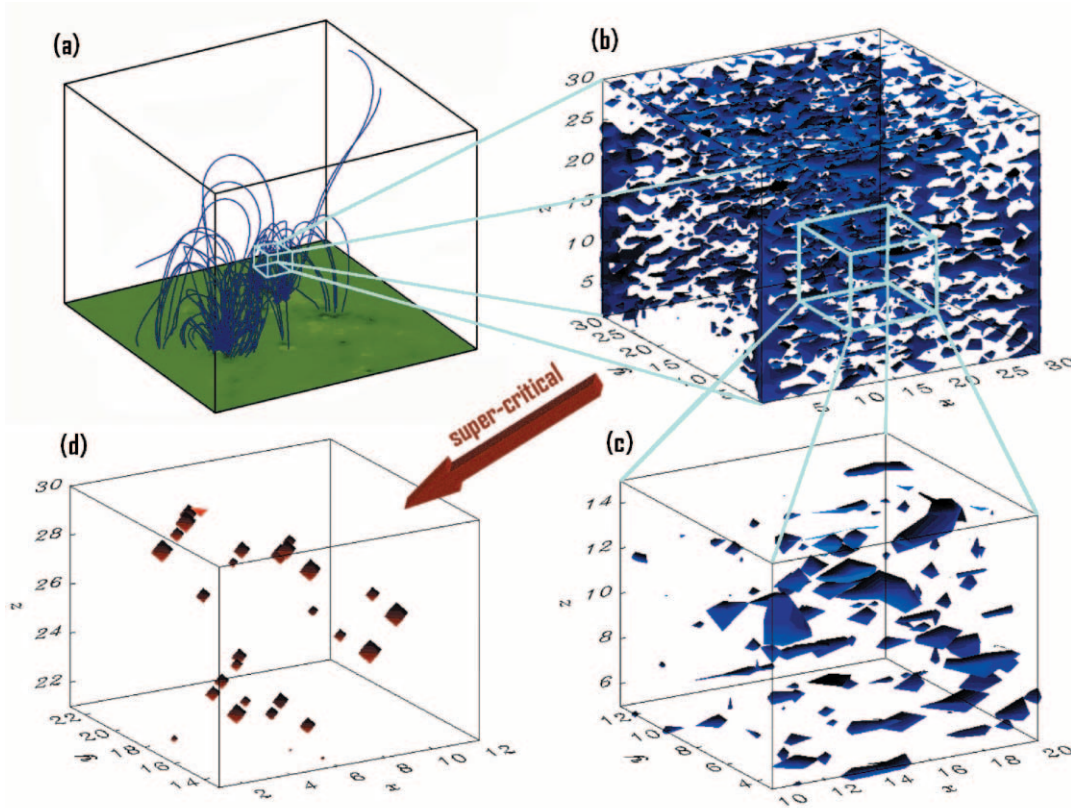


FIG. 1.—(a) Simulated magnetogram of a photospheric active region and force-free magnetic field lines, extrapolated into the corona (generated by the model of Fragos et al. 2004). (b) Subcritical current isosurfaces in space, as yielded by the X-CA model, which models a subvolume of a coronal active region. (c) Same as (b), but zoomed. (d) Temporal snapshot of the X-CA model during a flare, showing the spatial distribution of the UCS (supercritical current isosurface) inside the complex active region. The UCS form a fractal, and they are connected through large-scale magnetic field lines. The connectivity between the UCSs is an important ingredient of the acceleration mechanism proposed.

the problem along the path of our modeling approach. A conclusion is presented in § 5.

2. THE MODEL

In the model we propose in this paper, a three-dimensional large-scale magnetic topology, close to the structures estimated by force-free extrapolations of the photospheric magnetic fields, is the backbone of the system (see Fig. 1a). The magnetic field lines are the carriers of the high-energy particles. The UCSs, which basically are magnetic discontinuities, appear sporadically inside the large-scale magnetic topology, and they represent the dissipation areas of the turbulent system (see Fig. 1d). The characteristics of the UCS, such as size, energy content, etc., are different from UCS to UCS, following probabilistic laws that, in principle, should be dictated by the data; most of them, however, are not directly observable. The UCSs are assumed to be small-scale regions, distributed over space in a complex way. We thus implement the scenario of fragmented energy release, based on Parker's original conjecture (Parker 1988) and on the observational evidence of fragmentation in radio spike emission (see, e.g., Benz 2003), and in type III radio emission (e.g., Benz 1994).

One way of modeling the appearance, disappearance, and spatial organization of UCSs inside a large-scale topology is with the use of the extended cellular automaton (X-CA) model (Islsker et al. 1998, 2000, 2001). Figure 1 illustrates some basic features of the X-CA model.

The X-CA model has as a core a cellular automaton model of the sand-pile type and is run in the SOC state. It is extended

to be fully consistent with MHD: the primary grid variable is the vector potential, and the magnetic field and the current are calculated by means of interpolation as derivatives of the vector potential in the usual sense of MHD, guaranteeing $\nabla \cdot \mathbf{B} = 0$ and $\mathbf{J} = (c/4\pi) \cdot \nabla \times \mathbf{B}$ everywhere in the simulated three-dimensional volume. The electric field is defined as $\mathbf{E} = \eta \mathbf{J}$, with η the resistivity. The latter is usually negligibly small, but if a threshold in the current is locally reached ($|\mathbf{J}| > J_{cr}$), then current-driven instabilities are assumed to occur, η becomes anomalous in turn, and the resistive electric field locally increases drastically. These localized regions of intense electric fields are the UCSs in the X-CA model.

The X-CA model yields distributions of total energy and peak flux that are compatible with the observations. The UCSs in the X-CA form a set that is highly fragmented in space and time; the individual UCSs are small-scale regions, varying in size and are short-lived (see Fig. 1d). They do not form in their ensemble a simple large-scale structure but form a fractal set with fractal dimension roughly $D_F = 1.8$ (H. Islsker & L. Vlahos 2003, unpublished; McIntosh et al. 2002). The individual UCSs also usually do not split into smaller UCSs, but they trigger new UCSs in their neighborhood, so that different chains of UCSs travel through the active region, triggering new side-chains of UCSs on their way.

Following the picture we have from the X-CA model, we consider in this paper that the UCSs act as nodes of activity (localized accelerators) inside a passive three-dimensional large-scale magnetic topology. The UCSs are short-lived and appear randomly inside the large-scale magnetic topology

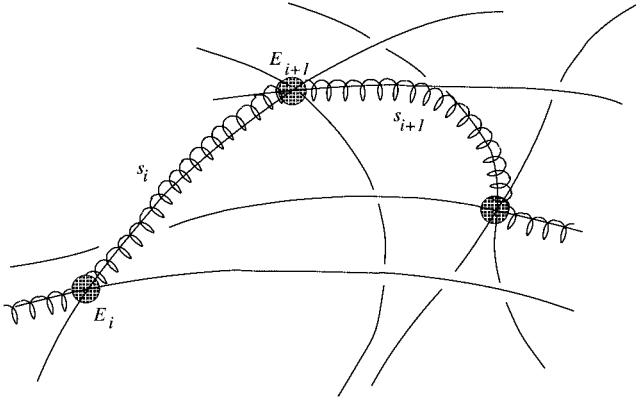


FIG. 2.—Sketch of the basic elements of the considered model. A particle (spiral line) basically follows the magnetic field lines (solid lines), although also undergoing drifts, and travels in this way freely a distance s_i , until it enters a UCS (filled circles), where it is accelerated by the associated effective DC electric field E_{i+1} . After the acceleration event, the particle again moves freely until it meets a new UCS.

when specific conditions for instability are met. The sketch in Figure 2 illustrates the situation.

Modeling this dynamic accelerator requires the knowledge of three probability density functions:

1. The probability density $P_1(s)$ defines the distances a charged particle travels freely in between two subsequent encounters with a UCS. The series of distances $s_1^{(j)}, s_2^{(j)}, \dots, s_n^{(j)}, \dots$, generated by the probability density $P_1(s)$, characterizes the trajectory of the j th particle in space. Every particle follows a different characteristic path.

The probability density $P_1(s)$ relates the particle acceleration process to the large-scale topology by implicitly representing the effects of the topology (the magnetic topology itself does not appear explicitly in the model). This aspect was not taken into account in previous acceleration models.

2. The probability density $P_2(E)$ provides the effective electric field $E_i^{(j)}$ acting on the j th particle for the effective time $\tau_i^{(j)}$ it spends inside the i th UCS. Particles follow very complicated trajectories inside the UCS. They may be accelerated by more than one acceleration mechanisms, but what is actually important for our model is the final outcome, i.e., we characterize a UCS as a simple input-output system, in which an effective DC electric field is acting. We thus assume that the effective action of a UCS is to increase a particle's momentum by $\Delta \mathbf{p}_i^{(j)} = e \mathbf{E}_i^{(j)} \tau_i^{(j)}$.

3. Finally, for the third probability, we have two alternatives: either we give the probability density $P_{3a}(\tau)$ of the effective times $\tau_i^{(j)}$ a UCS interacts with a charged particle, or we prescribe the probability density $P_{3b}(\ell)$ of the effective acceleration lengths $\ell_i^{(j)}$, i.e., the lengths of the trajectories along which the particles are accelerated.

The probabilities P_1 , P_2 , and P_3 (either P_{3a} or P_{3b}) are actually dependent on time. They must be assumed to change in the course of a flare, reflecting the changes in the overall density and connectivity of the UCS; the flaring active region is an evolving network of UCSs, whose instantaneous state determines the instantaneous intensity of the flare. However, we concentrate in our modeling on a short time during a flare, typically 1 s, so that we can assume that the state of the active region does not change significantly, and P_1 , P_2 , and P_3 can be considered independent of time. We show next that the above

probabilities define the charged particle dynamics inside the flaring region.

2.1. Charged Particle Dynamics

The particle j starts with initial momentum $\mathbf{p}_0^{(j)}$ from the initial position $\mathbf{r}_0^{(j)} = 0$ at time $t = 0$. The initial momentum $\mathbf{p}_0^{(j)}$ is such that the corresponding velocity $|\mathbf{v}_0^{(j)}|$ is drawn at random from the tail of a Maxwellian, $|\mathbf{v}_0^{(j)}| \geq v_{th}$, with v_{th} the thermal velocity. The particle is assumed to find itself in the neighborhood of a UCS at time $t = 0$, enters it immediately, and undergoes a first acceleration process.

During an interaction with a UCS, the particle's momentum evolves, in principle, according to

$$\frac{d\mathbf{p}^{(j)}}{dt} = e\mathbf{E} + \frac{e}{c}\mathbf{v}^{(j)} \times \mathbf{B}, \quad (1)$$

where $\mathbf{p}^{(j)} = \gamma m \mathbf{v}^{(j)}$ is the particle's relativistic momentum [$\gamma = 1/(1 - v^2/c^2)^{1/2}$, with $v = |\mathbf{v}^{(j)}|$], e is the charge of the particle, and c is the speed of light. Inside the UCSs, \mathbf{E} and \mathbf{B} are complex functions of time along the particle's complex trajectory. We thus average—in a loose sense—equation (1) over many internal trajectories in a given UCS, assuming that the corresponding averages exist:

$$\frac{d\langle \mathbf{p} \rangle}{dt} = e\langle \mathbf{E} \rangle + \frac{e}{c}\langle \mathbf{v} \times \mathbf{B} \rangle. \quad (2)$$

$\langle \mathbf{E} \rangle$ is now constant in a given UCS, and assuming that \mathbf{B} and above all v vary wildly in direction, so that $\langle \mathbf{v} \times \mathbf{B} \rangle = 0$ is a reasonable assumption, leads to

$$\frac{d\langle \mathbf{p} \rangle}{dt} = e\langle \mathbf{E} \rangle, \quad (3)$$

and we have reduced the UCS to a simple constant DC electric field device. Equation (3) is of course a strong simplification of the internal UCS physics; it actually implies that we treat the UCSs as black boxes, concentrating just on the statistical law of how the output is related to the input. The electric field $\langle \mathbf{E} \rangle$ must consequently be considered as an *effective* electric field, which summarizes the complex effects of shock waves, turbulence, and true DC-electric fields that must be expected to appear in and at a UCS (see § 1).

The effective electric field is constant in a UCS, as mentioned; it is assumed, however, to vary from UCS to UCS in a stochastic way, as prescribed by the probability density $P_2(E)$, where E is the magnitude of the effective electric field $\langle \mathbf{E} \rangle$.

After all, during the interaction with the i th UCS, a particle's momentum increases from $\mathbf{p}_i^{(j)}$ to $\mathbf{p}_{i+1}^{(j)}$ according to

$$\mathbf{p}_{i+1}^{(j)} = \mathbf{p}_i^{(j)} + e\langle \mathbf{E}_i \rangle \cdot \tau_i^{(j)}, \quad (4)$$

where $\langle \mathbf{E}_i \rangle$ is generated by the probability density $P_2(E)$. To determine $\tau_i^{(j)}$, we have two options in the model. In the first case, we directly generate $\tau_i^{(j)}$ from the probability density $P_{3a}(\tau)$. In the second case, the primary random variable is the acceleration length $\ell_i^{(j)}$, which is generated by the probability density $P_{3b}(\ell)$, and $\tau_i^{(j)}$ is derived under the assumption that the particle performs a relativistic, one-dimensional motion along the electric field of magnitude $E_i^{(j)}$ and length $\ell_i^{(j)}$, with initial momentum the magnitude of the total momentum $p_i^{(j)}$ the particle has before entering the UCS. In this

second case then, the time a particle spends inside a UCS is reduced when the particle's velocity increases.

After the particles has left the UCS, it performs a free flight until it again meets a UCS and undergoes a new acceleration process (see Fig. 2). The probability density $P_1(s)$ determines the spatial distance $s_i^{(j)}$ the particle travels before it meets this next UCS, situated at

$$\mathbf{r}_{i+1}^{(j)} = \mathbf{r}_i^{(j)} + s_i^{(j)} \hat{\mathbf{r}}_{i+1}^{(j)}, \quad (5)$$

where $\hat{\mathbf{r}}_{i+1}^{(j)} \equiv \mathbf{p}_{i+1}^{(j)} / |\mathbf{p}_{i+1}^{(j)}|$ is a unit vector into the direction of the free flight, and $\mathbf{r}_i^{(j)}$ is the location of the previous UCS the particle had met. Note that the spatial displacement a particle undergoes inside a UCS is neglected, corresponding to our assumption that the UCS are small-scale regions of negligible extent.

We keep track of the time passed during the acceleration process and the free flight,

$$t_{i+1}^{(j)} = t_i^{(j)} + \tau_i^{(j)} + s_i^{(j)} / v_{i+1}^{(j)}, \quad (6)$$

where $t_{i+1}^{(j)}$ is the time when the particle enters the $i + 1$ th UCS.

The particle starts a new cycle of acceleration and free flight at this point; the process as a whole is a cyclic one with continued probabilistic jumps in position- and momentum-space. In this paper, we monitor the system for times that are relatively short, on the order of 1 s. For such times, the particles can be assumed to be trapped inside the overall acceleration volume $V_{\text{acc}} = L_{\text{acc}}^3$, an assumption that will be confirmed by the results we present below in § 3. We thus do not have to include in the model the loss of particles that leave the active volume.

Let us now define the probability densities P_1 , P_2 , P_3 used in this study.

The probability density $P_1(s)$ of jump increments.—The active flaring region may be assumed to be in the state of MHD turbulence, embedded in a complex, large-scale magnetic topology. We claim that the UCSs, i.e., the regions of dissipation, are distributed in such a way that they form in their ensemble a fractal set. This claim is based on two facts:

1. Flaring active regions have successfully been modeled with SOC (see, e.g., Lu & Hamilton 1991; Lu et al. 1993; Isliker et al. 2000, 2001). It was demonstrated in Isliker et al. (1998, 2000, 2001) that the unstable sites in the SOC models represent actually small scale current dissipation regions, i.e., they can be considered as UCS. Furthermore, McIntosh et al. (2002) and H. Isliker & L. Vlahos (2003, unpublished) have shown that the regions of dissipation in the SOC models at fixed times form a fractal, with fractal dimension roughly $D_F = 1.8$.

2. From investigations on hydrodynamic turbulence we know that the eddies in the inertial regime have a scale-free, power-law size distribution, making it plausible that at the dissipative scale a fractal set is formed, and indeed, different experiments let us conclude that the dissipative regions form a fractal with dimension around 2.8 (see Anselmet et al. 2001 and references therein).

The particles in our model are thus assumed to move from UCS to UCS, the latter being distributed such that they form a fractal set. Isliker & Vlahos (2003) analyzed the kind of random walk where particles move in a volume in which a fractal resides, usually traveling freely but being scattered (accelerated) when they encounter a part of the fractal set. They

showed that in this case the distribution of free travel distances s in between two subsequent encounters with the fractal is distributed in good approximation according to

$$p(s) \propto s^{D_F-3} \quad (7)$$

as long as $D_F < 2$. For $D_F > 2$, $p(r)$ is decaying exponentially. Given that a dimension D_F below 2 is reported for SOC models, as stated above, we are led to assume that $P_1(s)$ is of power-law form, with index between -1 and -3 , preferably near a value of $D_F - 3 = -1.2$ (with $D_F = 1.8$, according to H. Isliker & L. Vlahos 2003, unpublished; McIntosh et al. 2002). Not included in the study of Isliker & Vlahos (2003) are two effects, (1) that the particles do not move on straight line paths in between two subsequent interactions with UCS, but they follow the bent magnetic field lines, and (2) that particles can be mirrored and trapped in some regions, making in this way the free travel distances larger. It is thus reasonable to consider the power-law index of $P_1(s)$ as a free parameter.

After all, we assume that the freely traveled distances s are distributed according to

$$P_1(s) = A s^{-a}, \quad \text{with } l_{\min} < s < l_{\max}, \quad (8)$$

where $l_{\min}(L_{\text{acc}})$ and $l_{\max}(L_{\text{acc}})$ are related to the characteristic length of the coronal active region L_{acc} , and A is a normalization constant.

The probability density $P_2(E)$ of effective electric fields.—The second probability density determines the effective electric field attached to a specific UCS. Its form should, in principle, be induced from a respective study, either from observations, which is not feasible so far, or from the simulation and modeling of a respective set-up, which to our knowledge seems not to exist to date. We are thus forced to try large classes of distributions. Two cases of distributions are definitely of particular interest, the ‘‘well-behaved’’ case, in which P_2 is Gaussian, and the ‘‘ill-behaved’’ case, in which P_2 is of power-law form. The Gaussian case is well behaved in the sense that all the moments are finite, and it is a reasonable choice because of the central limit theorem, which suggests Gaussian distributions if the electric field is the result of the superposition of many uncontrollable, small processes. The power-law case is ill-behaved in the sense that the moments on from a certain order (depending on the power-law index) are infinite. It represents the case of scale-free processes, as they appear for instance in SOC models. A characteristic of power-law distributions is the importance of the tail, which, in fact, causes the dominating effects.

Trying also the case of Gaussian distributions and guided by the results, we present in this study only the case in which the distribution of the electric field's magnitude is of power-law form,

$$P_2(E) = B E^{-b}, \quad \text{with } E_{\min} < E < E_{\max}, \quad (9)$$

which shows better compatibility with the observations. We note that most acceleration mechanisms mentioned earlier have power-law probability distributions for the driving quantity. Here $E_{\min}(E_D)$ and $E_{\max}(E_D)$ are related to the Dreicer field E_D , and B is the normalization constant. The Dreicer field is the electric field that leads an electron with initial velocity equal to the thermal velocity to unlimited acceleration (assuming that only Coulomb collisions can provide the energy losses), and for typical solar parameters it is $\sim 10^{-2} \text{ V m}^{-1}$.

Assuming, however, an anomalous collision frequency due to the presence of low-frequency waves or of turbulent magnetic fields, E_D increases dramatically by several orders of magnitude. We note that choosing the Dreicer field as a reference value is somewhat arbitrary; we might as well have used a typical coronal convective electric field. The effective electric field is then determined as $\langle E \rangle = E\hat{r}$, where \hat{r} is a three-dimensional unit vector in a completely random direction.

The probability densities $P_{3a}(\tau)$ and $P_{3b}(\ell)$ of effective acceleration times and lengths, respectively.—To complete the description of the acceleration process, we have two choices: to prescribe either the acceleration lengths or the acceleration times. For either of these distributions a model would be needed. However, since the acceleration times and lengths appear only in combination with the electric fields in the momentum increment, $e\langle \mathbf{E}_i^{(j)} \rangle \cdot \tau_i^{(j)}$ (see eq. [4]); the acceleration lengths come in indirectly), we can absorb any non-standard feature, such a scale-freeness or other strong non-Gaussianities, in the distribution of E . This is also reasonable since all three, τ , ℓ , and E , are effective quantities.

We thus assume in the first variant of the model that the time a particle spends inside a UCS obeys a Gaussian distribution with mean value τ_c and standard deviation τ_m ,

$$P_{3a}(\tau) = C_a e^{-[(\tau - \tau_c)^2 / 2\tau_m^2]}. \quad (10)$$

In the second variant, we prescribe the distribution of the acceleration lengths, and the acceleration times are calculated as secondary quantities. Again, a Gaussian distribution is assumed,

$$P_{3b}(\ell) = C_b e^{-[(\ell - \ell_c)^2 / 2\ell_m^2]}, \quad (11)$$

with mean ℓ_c and standard deviation ℓ_m . Defined in this way, the acceleration times or lengths are not essential for the acceleration process, although they influence the overall acceleration timescale, i.e., the global timing of acceleration.

It should be noted that the effective acceleration length, which is the length of the part of the internal trajectory along which a particle is accelerated, is very unlikely to be just equal to the linear size of the UCS, since a rather complex internal trajectory must be expected inside and near the UCS, including phenomena like trapping at the UCS and reinjection. Thus, the distribution of acceleration lengths used in our model does not give insight into the size distribution of the UCS. The acceleration times, on the other hand, can be compared to observed phenomena (see § 4). Yet, prescribing the acceleration lengths causes that the faster a particle is, the less time it spends in the acceleration events, which is physically reasonable.

Equations (4)–(11) allow one to follow the evolution of charged particles inside an evolving network of UCSs. Our main interest in the simulations that we present is to follow the evolution of the distribution in kinetic energy [$E_{\text{kin}} = (\gamma - 1)mc^2$] as a function of time. Therefore, we monitor the kinetic energies of the particles at prefixed times and construct their distribution functions $p(E_{\text{kin}}, t)$ (normalized to 1).

HXR bremsstrahlung.—We assume that the distribution $p(E_{\text{kin}}, t)$ of particles, as it is formed at time t , precipitates onto lower layers of the solar atmosphere, where it emits bremsstrahlung while being completely thermalized. As usual, we assume thick-target bremsstrahlung. The HXR emission spectra are calculated by using the formalism of Brown (1971),

according to which the photon count rate $I(\epsilon)$ (photons of energy ϵ per unit time and unit energy range) is calculated through an integral over the flux $F(E_{\text{kin}}, t)$ of precipitating electrons, which we determine as

$$F(E_{\text{kin}}, t) = n_1 p(E_{\text{kin}}, t)v + n_0 p_{\text{th}}(E_{\text{kin}})v, \quad (12)$$

where v is the velocity corresponding to E_{kin} , $p(E_{\text{kin}}, t)$ is given from the simulations in numerical form, $p_{\text{th}}(E_{\text{kin}})$ is the (normalized to 1) thermal distribution, taken in analytical form; n_1 is the number density of the precipitating electrons, and n_0 is the respective density of the background plasma. To complete the necessary parameters, an emitting area A also has to be specified.

The integration is done numerically. Since $p(E_{\text{kin}}, t)$ is given numerically at a relatively low number of discrete points—we typically use 30 bins in making the histograms—we use the values of $p(E_{\text{kin}}, t)$ at the midpoints of the bins and interpolate with cubic splines, which allows for precise enough numerical integration. The interpolation is done in the log-log, since we let the bin size increase with energy in order to reduce the statistical errors at high energies. Interpolating in the linear would lead to strong oscillations at high energies, whereas interpolation in the log-log is well behaved and follows smoothly the numerically given data points. Note that since the particle energy distributions depend on time, we also get time-dependent HXR spectra, $I(\epsilon, t)$.

Gyrosynchrotron microwave emission.—During their free flights, the particles gyrate in the background magnetic field and emit synchrotron radiation. Assuming a constant magnetic field B_0 and a homogeneous source region, we determine the gyrosynchrotron radiation spectra $F_O(\nu)$ and $F_X(\nu)$, which are the fluxes (in SFU) of the O - and X -modes, respectively.

The respective formulae, including the expressions for the emissivities and the absorption coefficients, are taken from Benka & Holman (1992) and are ultimately based on the work of Ramaty (1969). The evaluation of these formulae involve integrals over the distribution $p(\gamma)$ of the relativistic γ and its first derivative. Our model yields the distribution of kinetic energies $p(E_{\text{kin}})$ in numerical form, which we first transform into the distribution of γ according to $p(\gamma) = p(E_{\text{kin}})dE_{\text{kin}}/d\gamma$. The resulting $p(\gamma)$ is then given in numerical form at discrete γ -values. To integrate over $p(\gamma)$ and to calculate its derivative, we interpolate $p(\gamma)$ with cubic splines in the log-log, exactly as we did with $p(E_{\text{kin}}, t)$ in the case of the HXR emission described above. The differentiation is done by directly differentiating the interpolating spline polynomials.

To completely determine the emission, we need to specify the emitting area A , the thickness of the source d , and finally the angle θ_0 between the magnetic field and the line of sight. The frequency range for which the fluxes are calculated is chosen in the microwaves such that it corresponds to the typical observational range of current instruments.

3. RESULTS

The simulations are performed by using 10^6 particles (electrons, and in § 3.3 protons), and the system is monitored for 1 s, with the aim to concentrate our analysis on a short time-interval during the impulsive phase (for longer times we would have to include the explicit loss of particles from the accelerating volume). We performed an extended parametric study, of which we present here only one particular case; some general comments on the parameter dependence of the model

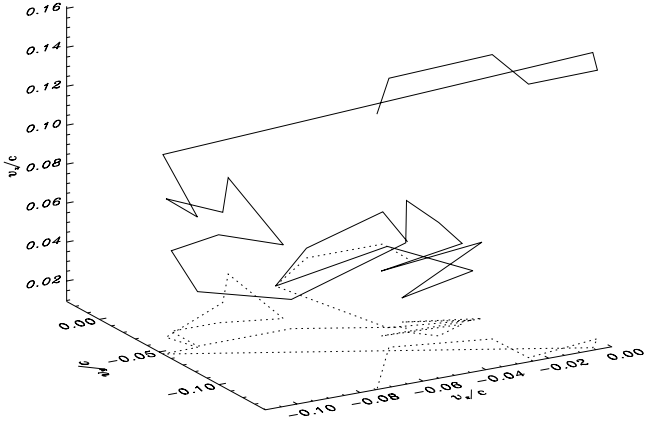


FIG. 3.—Particle trajectory in v -space (solid line), together with its projection onto the bottom (v_x - v_y) plane (dotted line). The velocities are in units of the speed of light c .

are made in § 4. The applied parameters for the case presented here are as follows:

Background plasma parameters.—We assume a temperature $T \approx 1.2 \times 10^6$ K (corresponding to 100 eV) and a density $n_0 = 10^{10}$ cm $^{-3}$ for the ambient, background plasma. To estimate the synchrotron losses, a background magnetic field $B_0 = 100$ G is assumed. For the calculation of the HXR emission, we use again the aforementioned values of the background plasma temperature T and density n_0 , and we moreover assume an emitting area $A = 10^{18}$ cm 2 and a density of accelerated particles $n_1 = 2 \times 10^7$ cm $^{-3}$. The same parameters B_0 , n_0 , n_1 , and A are applied in the calculation of the gyro-synchrotron emission, together with a thickness of the emitting region $d = 10^9$ cm and an angle $\theta_0 = 45^\circ$ between the magnetic field and the line of sight.

Random walk in position space.—This is characterized by the power-law exponent $a = 1.2$ and by the minimum and maximum jump lengths $l_{\min} = 10^{-6}L_{\text{act}}$ and $l_{\max} = 10^3L_{\text{act}}$, with $L_{\text{act}} = 10^{10}$ cm (see eq. [8]).

Electric field statistics.—The power-law index of the electric field distribution is set to $b = 4.5$, and we choose the range from $E_{\min} = E_D$ to $E_{\max} = 10^8E_D$, where the Dreicer field E_D is a function T and n_0 (see eq. [9]).

Effective acceleration times and lengths.—Either the acceleration times or the acceleration lengths are prescribed. The Gaussian of the acceleration times is determined by the mean value $\tau_c = 2 \times 10^{-3}$ s and the standard deviation $\tau_m = \frac{2}{3} \times 10^{-3}$ s (see eq. [10]), whereas the Gaussian of the acceleration lengths has mean value $\ell_c = 5 \times 10^7$ cm and standard deviation $\ell_m = (5/3) \times 10^7$ cm (see eq. [11]); we note that the acceleration lengths cannot be directly compared to the UCS sizes, see § 2.1].

3.1. Electron Diffusion Inside the Network of UCS

Up to the 1 s that we monitor the system, the electrons repeatedly undergo acceleration events, the number of which differs from particle to particle; for the variant of the model with the acceleration times prescribed, the minimum number of acceleration events per particle is found to be 1, the maximum is 175, and the mean is 13.4. We thus have quite a low mean number of acceleration events, and a fraction of the particles undergoes just one initial acceleration process. Figure 3 shows a particle trajectory in velocity space. Characteristic is the appearance of jump lengths of various sizes, from small to

large, which is a consequence of the power-law form of the momentum increment (see eqs. [4] and [9]), and it is actually a typical property of Levy walks. We do not show a position-space trajectory, since it is difficult to visualize. The increments are again power-law distributed (eq. [8]), albeit with very low index (1.2), implying that there occur very large increments; in a plot only the largest increment will be seen as a straight line, and the smaller increments are not resolved.

To analyze the diffusive behavior of the electrons in position space, we determine the mean square displacement $\langle r^2(t) \rangle$ of the particles from the origin as a function of time, and the result is presented in Figure 4 for the case in which the acceleration times are prescribed. For all times that the system is monitored, we find strong superdiffusion, $\langle r^2(t) \rangle \propto t^\gamma$, with γ between 2.3 and 3.2. The behavior is different above and below 4×10^{-3} s, a time that is related to the acceleration time: at $\tau_c + 3\tau_m = 4 \times 10^{-3}$ s, the vast majority of the particles have finished their first acceleration process (since the acceleration times are Gaussian-distributed [see eq. (10)], 99% of the particles have an acceleration time smaller than the time of 3 standard deviations above the mean value). Below 4×10^{-3} s, the particles are typically still in their first acceleration process, whereas above 4×10^{-3} s, some particles are on free flights and others are in new acceleration processes. We cannot claim that the diffusive behavior has settled to a

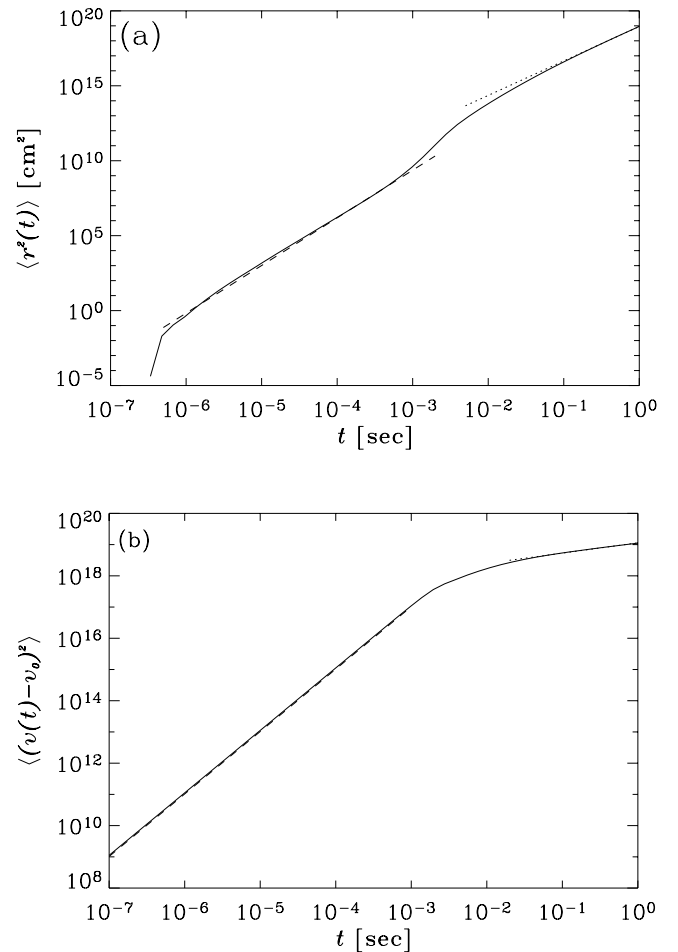


FIG. 4.—Diffusive behavior for the case in which the acceleration times are prescribed. (a) $\langle r^2(t) \rangle$ vs. t , together with two reference lines of slope 3.18 (dashed line) and 2.30 (dotted line), respectively. (b) $\langle (v(t) - v_0)^2 \rangle$ vs. t , with again two reference lines of slope 2.00 (dashed line) and 0.33 (dotted line), respectively.

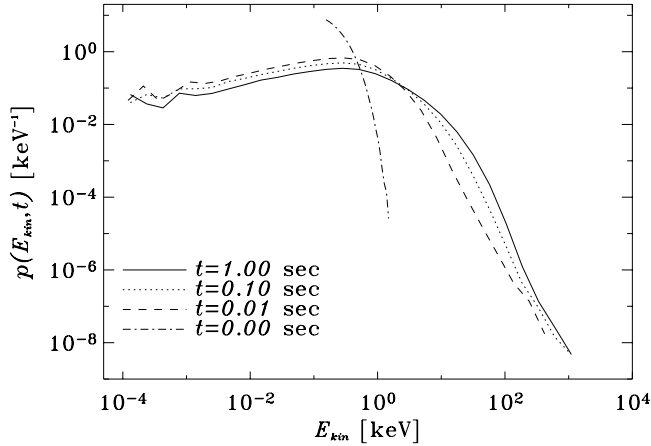


FIG. 5.—Kinetic energy distributions $p(E_{\text{kin}}, t)$ (probability density function, normalized to 1) at times $t = 0, 0.01, 0.1, 1$ s, for the case in which the acceleration times are prescribed.

stationary behavior in the 1 s that we monitor the system. At 1 s, we find $\langle r^2(t = 1 \text{ s}) \rangle \approx 10^{19} = L_{\text{act}}^2/10$, and the particles have diffused a distance less than the active region size, so that we do not have to worry about losing particles by drifting out of the active region, as claimed earlier.

We next analyze the diffusive behavior in velocity space, determining the mean-square displacement $\langle (v(t) - v_0)^2 \rangle$ of the particles from their initial velocity v_0 . Figure 4 shows the result. The particles start with $\langle (v(t) - v_0)^2 \rangle \propto t^{2.00}$ until roughly 0.001 s, a time slightly earlier than τ_m , the mean acceleration time. This reflects the fact that basically all particles are still in their first acceleration event, and their velocity evolves according to $v(t) \propto (eE/m)t^2$. For larger times, $\langle [v(t) - v_0]^2 \rangle$ starts to turn over, and in the range from 0.02 to 1 s, where all the particles have finished their first acceleration event, we find $\langle [v(t) - v_0]^2 \rangle \propto t^{0.33}$. The system exhibits thus clear subdiffusive behavior in velocity space (corresponding to the nonrelativistic energy space).

3.2. Kinetic Energy Distribution, Microwave, and HXR Emission

At pre-fixed times, we collect the kinetic energies of the electrons and construct their histograms, which, normalized to 1, yield the kinetic energy distributions $p(E_{\text{kin}}, t)$, shown in Figure 5 for the case with prescribed acceleration times. The distributions remain of similar shape for the time period monitored, exhibiting a flatter part at low energies, and a power-law tail above roughly 5 keV. The low-energy part is actually of a Maxwellian type. The power-law index of the high-energy tail varies around 4, increasing slightly with time, and the particles also reach higher energies with increasing time. We thus see a systematic shift of the Maxwellian toward higher energies, with in parallel the development of a power-law tail extending to higher and higher energies and steepening. At 1 s, the most energetic particles have reached kinetic energies slightly above 1 MeV. If we define the approximate power-law tail somewhat arbitrarily to start at 5 keV, we find that roughly 35% of the electrons are in the tail at $t = 1$ s. The results for the case in which we prescribe the acceleration lengths are qualitatively similar, although the power-law tail is steeper, with a power-law index around 5.

During their free flights, the particles move in a constant background magnetic field; they thus gyrate and emit synchrotron radiation. The microwave spectrum for both the

X -mode $[F_X(\nu)]$ and the O -mode $[F_O(\nu)]$ is calculated according to § 2.1, and Figure 6 shows the spectra for the case in which the acceleration times are prescribed. Besides some fluctuations at low frequencies, the spectra exhibit an increase with frequency, a turnover, and a decrease toward high frequencies. The turnovers for the X - and O -modes are slightly different, as are the low-frequency cutoffs. The degree of polarization can reach values up to 60%.

Next, we let the electron populations, as they are formed at different, prescribed times, precipitate onto lower layers of the solar atmosphere. Figure 7a shows the bremsstrahlung emission spectra as a function of time, calculated according to § 2.1, and with the acceleration times prescribed. Note that Figure 7 shows only the electron contribution; not included are, in particular, the ion contribution, the nuclear lines, and the emission from particle annihilation. The lower cutoff in the photon count rate is chosen to correspond to the one of modern instruments, which typically observe power-law decays over 4 orders of magnitude in count rate before reaching the noise level (e.g., Lin et al. 2003). Below the cutoff, the simulated count rate falls fast off to zero.

For all times monitored, the spectra are of power-law shape, with a turnover and falloff to zero at the photon energy corresponding to the highest electron energy reached. The steepening below roughly 15 keV is the thermal emission of the background plasma. The spectral indices are all above 2, and they increase with time, with a value of 2.1 at $t = 0.01$ s and finally reaching 2.5 at 1 s (from a power-law fit above 10 keV).

In the case in which the acceleration lengths are prescribed, we find for $t = 0.01$ s a single power law with index 3.0, at $t = 0.1$ s an approximate double power law with spectral indices 1.9 at low and 4.3 at high energies, and finally for $t = 1$ s the double power law persists, with indices 1.7 at low energies and 4.7 at high energies (Fig. 7b). In the course of time, the power laws thus get flatter at low energies and steeper at high energies.

In addition, we checked the importance of synchrotron radiation losses for the particle dynamics during the free flights, assuming gyration in a constant, uniform magnetic field $B_0 = 100$ G. We found that the radiative losses do very insignificantly influence the results; they basically remain unaltered. The reason is that the magnitude of the magnetic field is not very large, and above all the free flight times are too short to allow substantial losses in energy.

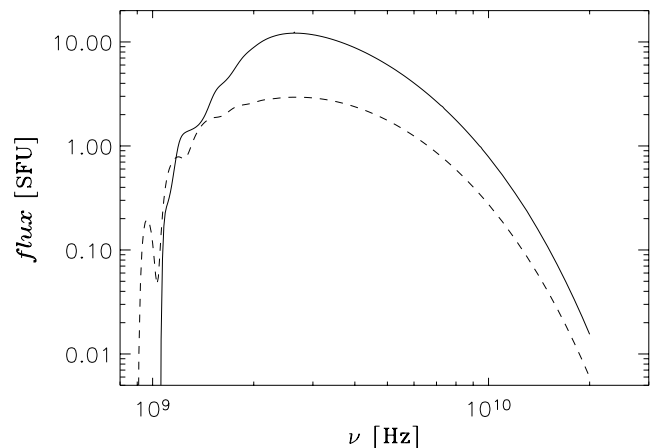


FIG. 6.—Microwave-emission spectrum (flux in SFU) at time $t = 1$ s. X -mode $[F_X(\nu)]$, solid line; O -mode $[F_O(\nu)]$, dashed line.

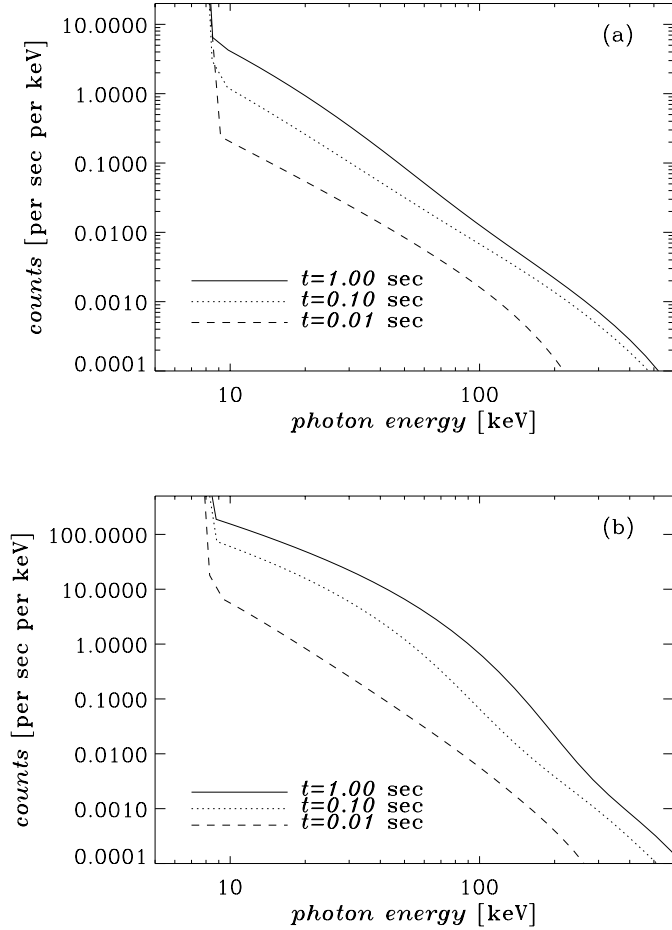


FIG. 7.—(a) HXR bremsstrahlung spectra for the times $t = 0.01, 0.1, 1$ s and with the acceleration times prescribed, derived from the corresponding kinetic energy distributions shown in Fig. 5, including thermal emission. (b) HXR spectra for prescribed acceleration lengths.

The kinetic energy distributions that the model yields are approximately Maxwellians with a power-law tail above roughly 1 keV (Fig. 5). Fitting a Maxwellian in the low-energy range from 0.01 keV up to roughly 0.5 keV yields the temperature of the thermal part of the distribution. We find for prescribed acceleration times that the population of electrons moving through the UCS is heated on very fast timescales (0.01 s) from the initial temperature of approximately 1.2×10^6 K to temperatures on the order of 6.6×10^6 K, around which it fluctuates until $t = 1$ s, without any significant further increase. However, we have to note that the Maxwellian does not fit perfectly; at low energies there is a systematic overpopulation. This is most likely because we do not include collisions, which would thermalize the distribution to an exact Maxwellian. Nevertheless, the temperatures inferred can be considered to be indicative of the heating process.

3.3. Acceleration and Heating of Ions

It is of interest to know what will happen to ions that go through the same kind of process as the electrons. To adjust our model to the case of ions, we only have to replace the electron mass with the ion mass. Keeping all the parameters fixed as described in the beginning of § 3 and using the variant of the model with prescribed acceleration times, we find in the case of protons that the initial distribution is basically unaltered, even for times such as 1000 s. The reason is that the

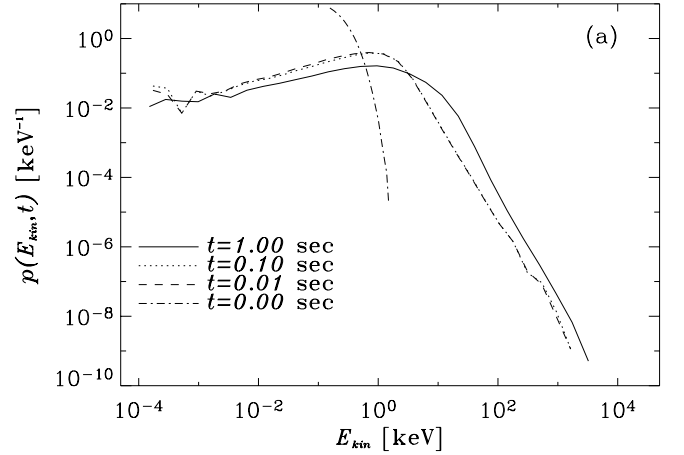


FIG. 8.—Kinetic energy distributions (normalized to 1) of protons at times $t = 0, 0.01, 0.1, 1$ s.

momentum increments are too small for the ions to undergo a visible change in energy distribution; they need larger momentum increments. There are several possibilities in the frame of our model to achieve larger momentum increments; the most straightforward ones are either to increase the acceleration times or increase the effective DC electric field.

In the case we show here, we increase the acceleration times by a factor of 100 compared to the electrons, leaving all the other parameters unchanged. We thus apply the mean value $\tau_c = 2 \times 10^{-1}$ s and the standard deviation $\tau_m = \frac{2}{3} \times 10^{-1}$ s in equation (10). Figure 8 shows the kinetic energy distributions. They exhibit a rough Maxwellian at low energies and a power-law tail with a slope increasing in time, reaching a value of roughly 3.2 at $t = 1$ s. The distributions for $t = 0.01$ and 0.1 s are similar, most likely since for these times most particles are still in their first acceleration process, which will have ended for almost all particles at the time $\tau_m + 3\tau_c = 0.4$ s (see the corresponding argument in § 3.1). The fraction of particles in the tail above 10 keV is 29% at $t = 1$ s. The Maxwellian part of the distributions is shifted to higher energies in the course of time, which corresponds to heating. Thus, the model also yields heating and acceleration of the protons.

We found similar results when adjusting the minimum of the electric field distribution to $E_{\min} = 100E_D$ (see eq. [9]), which increases the mean value of the effective electric field and causes in this way larger momentum increments for the protons. In the variant of the model with prescribed acceleration lengths, the ions are accelerated up to roughly 550 keV, without changing any parameter of the model.

4. DISCUSSION

The model we introduced is the general framework of any model of multiple particle acceleration; it is the most general approach in the sense that all kinds of multiple acceleration problems, not just the solar flare problem, can be cast into this general form by adjusting the elements appropriately.

The model is specified by setting the elements of the spatial random walk and the random walk in momentum space. Setting these elements should be done along the guideline of physical insight into the problem under study, an insight that comes from independent studies in different fields. The nature of the model partly implies that new kinds of questions should be asked in the different involved fields, stressing the statistical nature of different mechanisms and effects.

In the application to solar flares we present here, it is necessary to study the statistical properties of an isolated UCS, i.e., to investigate the statistics of the energy gain when an entire distribution of particle moves through a UCS, all particles having random initial conditions. This question belongs to the field of MHD in combination with kinetic plasma physics (which refers to anomalous resistivities). Also needed is an understanding of the spatial organization of an ensemble of coexisting UCSs and of their connectivity and evolution. A first hint as to how the UCSs might be spatially organized comes from the cited inquiries into SOC models, which favor a global fractal structure with dimension around 1.8. The problem actually concerns the nature of three-dimensional, large-scale, magnetized MHD turbulence, and it involves theory as well as observations.

With our concrete specifications of the combined random walk to the solar flare problem, we were able to achieve HXR spectra that are compatible with the observations. What is important is that the model naturally leads to heating of the plasma, or, more precisely, it creates a heated population in the plasma. This heated population can be expected to heat the entire background plasma through collisional interactions on collisional timescales, explaining in this way the observed delay between the thermal soft X-ray and the nonthermal HXR emission. This mechanism of heat diffusion, however, is not included in our model.

4.1. Diffusion

Position- and velocity-space diffusion of the particles is anomalous; the particles are highly superdiffusive in position space and subdiffusive in velocity space (Fig. 4). The position space superdiffusion implies that the particles move quickly through the active region. At 1 s, the particles have moved approximately a distance 3×10^9 cm $\approx L_{\text{act}}/3$, so that fast particle escape must be expected. The particles may either diffuse to open field line regions, from where they directly escape outward, eventually generating type III radio bursts, or they may diffuse toward the lower atmosphere and give rise to bremsstrahlung emission. This fast timescale of potential particle escape in the model is in qualitative accordance with the observed fast appearance of HXR emission and type III bursts in flares—a conclusion that we cannot draw too rigorously, however, since the free flight of the particles we assume in the model is a simplification, an explicitly introduced guiding magnetic field topology might introduce effects that could to some degree alter this result.

4.2. Parametric Study

We performed an extended parametric study of the model. The parameter space is quite high dimensional; the results are dependent not only on the power-law indices of the electric field and the spatial jump distributions, but also on the respective ranges ($I_{\text{min}}, I_{\text{max}}, E_{\text{min}}, E_{\text{max}}$), and finally on the mean value of the acceleration times (or acceleration lengths) and their standard deviation. As a rule, the model yields power-law and also double power-law tails with varying power-law indices and varying ranges in the kinetic energies, and also power-law-shaped HXR spectra. The problem is to find parameter ranges in which the spectral index is compatible with the observations.

The power-law index of the spatial jump distribution we used here is 1.2, corresponding to the case of fractally

distributed UCSs with fractal dimension 1.8, and thus being consistent with the results from SOC models (see § 2).

The power-law index of the electric field distribution is 4.5, a value we thus far cannot justify with physical arguments. Note, however, that the electric field used here is an effective one, and we are not aware of a study we could compare it to. Choosing the lower limit E_{min} of the electric fields as the Dreicer field is physically reasonable. Changes in E_{min} on the order of, say, 10% already influence the results quite strongly, above all with respect to the highest energies reached by the particles. We justify setting the maximum E_{max} of the electric fields to a relatively high value ($E_{\text{max}} = 10^8 E_D$) with the following argument: UCSs are characterized not least by an intense current, which is very likely to trigger some kinetic instabilities, with the result that the resistivity is drastically increased by several orders of magnitude, becoming anomalous; through Ohm's law, very strong electric fields must be expected to appear in the short times until the energy is dissipated.

The acceleration times are on the order of several milliseconds, a timescale that is roughly comparable to the fastest, nonthermal emissions observed in flares, the so-called narrowband, millisecond radio spikes emission (e.g., Benz 1986). The acceleration lengths, on the other hand, we do not consider to be directly comparable to observed phenomena, as explained in § 2.1.

Notably, we find cases in which power-law tails are developed; i.e., where we do find acceleration, the HXR emission is too weak to overcome the thermal emission. This finding favors the hypothesis that there is significant activity of small-scale heating and acceleration that is, however, impossible to observe in the HXR, since it is covered by the thermal emission.

After all, we cannot claim that we have found the only and unique set of parameter values for the problem under scrutiny; because of the complexity of the model, there may be other combinations of parameters that give results compatible with the observations. It seems, however, that the values we chose are quite physically reasonable. We plan to do a detailed parametric study, such as the HXR spectral index as a function of the electric field distribution power-law index, in a future paper.

4.3. Ions

Application of the model (in the variant with prescribed acceleration times) to ions yields results similar to the case of the electrons, as long as the mean acceleration time is increased or stronger electric fields are applied.

In the case of increased acceleration times, the process accelerating the ions and the electrons is assumed to be the same, but the ions move with a lower velocity. Assuming that ions and electrons have the same temperature, the initial velocities of the protons are on the order of $(m_e/m_p)^{1/2}$ times smaller than those of the electrons, where m_e and m_p are the electron and proton mass, respectively. The momentum increments in our model are independent of the masses, so that the corresponding increments in velocities are on the order of m_e/m_p times smaller for the protons than for the electrons. Assuming that the acceleration times are loosely related to $1/v$, where v is a typical particle velocity, i.e., the particles move along an internal trajectory in the UCS that is of similar length for electrons and protons, we find that the acceleration times must roughly be expected to be between $(m_p/m_e)^{1/2} \approx 42$ and

$m_p/m_e \approx 1 \times 800$ times larger for the protons than for the electrons. The 100 times larger proton acceleration times we applied in this paper are thus in a justifiable range of values.

The advantage of the variant of the model with prescribed acceleration lengths is that without adjustment of the parameters from the electron case, the ions get accelerated, albeit not to very high energies. The acceleration length variant has implicitly built in the mass-dependence of the acceleration efficiency.

4.4. Comparison to Observations

Benz and his collaborators have repeatedly stressed and discussed in detail the observational fact of fragmentation of the energy release (e.g., Benz 1994). They give evidence that the coronal acceleration region is probably cospatial with the decimetric spikes emitting volume (Benz 2003), which in turn is highly fragmented in space and time. Another observational result favoring the fragmentation of the acceleration region is the appearance of groups of type III bursts during the impulsive phase of flares (Benz 1994). Our model incorporates the scenario of fragmented energy release; it is actually one of its basic assumptions.

The observed nonthermal HXR spectra are characterized by a near power-law form (often double power-law), with a spectral index that varies in the course of a flare, which is, however, always clearly above 2, and which is anticorrelated with the HXR flux (e.g., Hudson & Fárník 2002; Krucker & Lin 2002; Lin et al. 2002; Saint-Hilaire & Benz 2002; Sui et al. 2002). According to Lin et al. (2003), the spectra up to 400 keV are generated purely by the electrons; from 400 keV to 1.4 MeV electron bremsstrahlung dominates, although ion emission starts increasingly to alter the spectra, and above 1.4 MeV the spectra are dominated by the ion line emission. The HXR spectra we presented are generated by electron bremsstrahlung; they extend up to 500 keV, and from their power-law shape and spectral index they can be considered compatible with the observations. Slight variations in the model parameters will be reflected in variations of the spectral index. In particular, the variant of the model in which the acceleration lengths are prescribed has a tendency to yield double power laws for larger times; it seems that the most energetic particles get less and less increase in energy as they become faster, leading to a steepening of the power-law tail. However, the double power law becomes too flat at low energies for too large times—actually, there the model in its current form reaches its limitations; it is constructed only for the very first period of the impulsive phase, since collisional losses and losses of particles out of the active region are not included.

The observed microwave emission seems not to follow a very clear, universal spectral shape. Usually, the spectrum increases until a frequency of a few hundred MHz, and then it falls off quite steeply, sometimes in a clear power-law form, sometimes in a more exponential manner (see, e.g., Lee et al. 2003; Fleishman et al. 2003). We can thus conclude that the microwave spectrum yielded by our model seems compatible with the observations. Note that the microwave spectra and the degree of polarization depend quite sensitively on the assumed background magnetic field strength B_0 . While the shape of the spectrum remains qualitatively the same, the steepness of the increase at low frequencies and of the decrease at high frequencies quantitatively change, their closeness to power-law shapes varies, and the turnover frequency and the relative

intensity of the O - and X -modes change, if the value of B_0 changes.

4.5. On the Number Problem

The number problem refers to the question of whether an acceleration mechanism is efficient and fast enough to generate the large number of accelerated particles as they are inferred from the observations. Miller et al. (1997 and references therein) mention that roughly 10^{34} – 10^{37} electrons s^{-1} are accelerated; the number cannot be very precise, as it is indirectly derived and depends on several assumptions on emission mechanisms and on mostly assumed active region parameters.

In order to check the efficiency of our model, we first numerically determine the total energy $E_{\text{kin},t}$ of the n_e electrons that are in the power-law tail, with n_e now a free parameter, $E_{\text{kin},t} = n_e \int_{5 \text{ keV}}^{E_{\text{max}}} p(E_{\text{kin}}, t = 1 \text{ s}) E_{\text{kin}} dE_{\text{kin}}$, where $p(E_{\text{kin}}, t = 1 \text{ s})$ is the numerically given kinetic energy distribution at $t = 1 \text{ s}$, as yielded by our model, and the tail is defined to start above 5 keV (see § 3.2 and Fig. 5). Integrating numerically, we find $E_{\text{kin},t} = n_e 9 \times 10^{-9}$ ergs. If we assume a large, but not huge, flare in which, say, 10^{30} ergs of energy are released during, say, 100 s, we find that $n_e \approx 10^{36}$ electrons s^{-1} must be accelerated. In a typical coronal active region of volume $L_{\text{acc}}^3 = 10^{30} \text{ cm}^3$ and with particle density $n_0 = 10^{10} \text{ cm}^{-3}$, there is a total number of 10^{40} particles. During the flare of 100 s duration, 10^{38} particles are accelerated in total and potentially leave, corresponding to 1% of the initial particles. With these numbers, it seems that there is no essential depletion of the flaring volume, and there is thus no need for a secondary mechanism of replenishment. We note that the volume assumed in this estimate is that of the entire active region, since the high diffusivity of the particles (see earlier in this section) and the nature of SOC (see Fig. 1) allow us to expect that the entire active region contributes to the acceleration of particles in flares.

Doing the same kind of analysis for the ions, with the difference that the power-law tail now starts above 10 keV (see Fig. 8), we find a total energy of the accelerated protons $E_{\text{kin},t}^{(i)} = n_e 1.0 \times 10^{-8}$ ergs (in the case of increased acceleration times; see § 3.3) or $E_{\text{kin},t}^{(i)} = n_e 2.5 \times 10^{-8}$ ergs (in the case of increased electric fields), which is roughly 1.1–3 times larger than the electron energy in the tail, so that fewer protons have to be accelerated to account for the observed energies. We note that this result does not imply an imbalance between electron and proton acceleration; there may well exist an unobserved, “dark” population of particles, above all protons at low energies, so that the numbers of accelerated electrons and protons may actually be equal.

4.6. Main Achievements of Our Model and Open Questions

The main results and characteristics of our model are as follows:

1. The acceleration process is extremely fast. Electrons reach MeV energies in 0.01 s, and ions approach 10 MeV in 1 s.
2. Our model exhibits strong superdiffusion of particles in position space. One important effect of the fast transport of accelerated particles is that they can be expected to reach fast open field-line regions. Accelerated particles will thus easily escape into the upper corona and the interplanetary space if closed and open field line regions coexist inside a large active region.

3. The energy spectra formed for both species are Maxwellians with steep power-law tails.

4. The HXR spectra are compatible with the observations (power-law shapes, spectral indices above 2).

5. The microwave spectra are qualitatively compatible with the observations.

6. We observe efficient, fast plasma heating. Energy release, acceleration, and heating are unified, they are the result of the same process.

7. The results for electrons and ions are quite similar; however, the ions need either longer acceleration times or stronger electric fields.

8. The total number of accelerated particles is compatible with numbers derived from observations.

9. Electrons and ions reach their maximum energy on a very fast timescale; the system adjusts itself quickly to the conditions imposed by the magnetic structure and the energy release process [in the model through the modification of the chosen probabilities $P_1(s)$, $P_2(E)$, $P_3(\tau)$; see § 2.1]. In other words, the acceleration would follow the evolution of $P_1(s, t)$ and $P_2(E, t)$ very closely; it instantaneously adjusts itself to the instantaneous coronal conditions.

We have shown that radiative losses due to synchrotron radiation are negligible for the particle dynamics as a result of the energies and the densities considered here, but in general they have to be incorporated in the evolution of particles, especially if this process is applied to astrophysical sources.

Not included in our study are the collisional losses of the particles during their free travels. They could possibly affect mainly the particles with low velocities; a fraction of the particles might be thermalized during their free flights. Also not included are the radiation associated with collisions, the possible thin target HXR emission of the system, and the escape of particles, i.e., the diffusive loss of particles out of the active region.

It should also be mentioned that in the random-walk approach we made here, the spatial evolution of the particles is treated in a simplified way; we have included the magnetic topology only implicitly through the distribution $P_1(s)$ of spatial jumps. An explicit inclusion of topology would cause effects like escape, mirroring, and trapping, which might affect the timing and the spatial structure of a flare to some degree (e.g., “loop-tops,” “loop-top with a helmet,” “footpoints,” etc.).

5. CONCLUSION

In this paper, we shifted the emphasis of the acceleration process in active regions away from the details of specific

mechanism(s) involved and focused on the global aspects of the active region, its evolution in space and time, and on the stochastic nature of the acceleration process. Our basic assumptions are as follows: (1) acceleration is a local process in and near the UCSs, (2) the UCSs are distributed in a complex way inside the large-scale three-dimensional magnetic topology of the active region, and (3) acceleration is the result of multiple interactions with different UCSs. These assumptions can be summarized in the statement that energy dissipation and particle acceleration in flares are fragmented. We are able for the first time to connect the accelerator to the three-dimensional magnetic topology and the energy release process. From our results, we can safely conclude that the complexity of the three-dimensional magnetic field topology in active regions, in combination with the stresses imposed by the convection zone onto it, forms a highly efficient accelerator.

The adequate tool for modeling the stochastic nature of particle acceleration in flares is a continuous-time random walk in position and velocity space. This new approach opens up the way for understanding a variety of acceleration phenomena, e.g., acceleration before and after a flare, acceleration without a flare, long-lasting acceleration, etc.

We feel that the road opened in this paper is new and still unexplored in astrophysics. As mentioned, it can provide answers to a number of open problems that have remained unsolved since researchers first attempted to use one UCS (above or inside a flaring loop) and one (uncorrelated with the energy release) acceleration mechanism to explain phenomena of acceleration. Many new questions are still open, and we plan to return to these issues in a forthcoming paper.

This work was supported in part by the Research Training Network (RTN) “Theory, Observation, and Simulation of Turbulence in Space Plasmas,” funded by the European Commission (contract HPRN-eT-2001-00310). The authors would like to thank A. Anastasiadis for helpful discussions and comments on the manuscript, and the referee for his constructive critique, which helped to improve the paper. T. Fragos, M. Rantziou, and I. Sandberg are acknowledged for their help in image processing. L. V. was a member of the team “Critical Problems in Solar Flare Physics,” which met three times during the period from 2000 to 2003. He is most grateful to the International Space Science Institute (ISSI) in Bern for supporting his participation. He is also grateful to the team members P. Cargill (team leader), Arnold Benz, Hugh Hudson, Brigitte Schmieder, and George Simnett for the stimulating discussions and constructive suggestions.

REFERENCES

- Albert, R., & Barabasi, A. L. 2002, *Rev. Mod. Phys.*, 74, 47
 Ambrosiano, J., Matthaeus, W. H., Goldstein, M. L., & Plante, D. 1988, *J. Geophys. Res.*, 93, 14383
 Anastasiadis, A., & Vlahos, L. 1991, *A&A*, 245, 271
 ———. 1994, *ApJ*, 428, 819
 Anastasiadis, A., Vlahos, L., & Georgoulis, M. 1997, *ApJ*, 489, 367
 Angelopoulos, V., Mukai, T., & Kokubun, S. 1999, *Phys. Plasmas*, 6, 4161
 Anselmetti, F., Antonia, R. A., & Danaila, L. 2001, *Planet. Space Sci.*, 49, 1177
 Arzner, K. 2002, *J. Phys. A*, 35, 3145
 Bak, P., Tang, C., & Wiesenfeld, K. 1987, *Phys. Rev. Lett.*, 59, 381
 Benka, S. G., & Holman, G. D. 1992, *ApJ*, 391, 854
 Benz, A. O. 1986, *Sol. Phys.*, 104, 99
 ———. 1994, *Space Sci. Rev.*, 68, 135
 ———. 2003, in *Energy Conversion and Particle Acceleration in the Solar Corona*, ed. K. L. Klein (Berlin: Springer), 80
 Blandford, R., & Eichler, D. 1987, *Phys. Rep.*, 154, 1
 Brown, J. C. 1971, *Sol. Phys.*, 18, 489
 Cargill, P. 2002, in *SOLMAG: Magnetic Coupling of the Solar Atmosphere*, ed. H. Sawaya-Lacoste (ESA SP-505; Noordwijk: ESA), 245
 Crosby, N. B., Aschwanden, N. J., & Dennis, B. R. 1993, *Sol. Phys.*, 143, 275
 Decker, R. B. 1988, *Space Sci. Rev.*, 48, 195
 Decker, R. B., & Vlahos, L. 1986, *ApJ*, 306, 710
 Dorogovtsev, S. N., & Mendest, J. F. F. 2002, *Adv. Phys.*, 51, 1079
 Ellison, D. C., & Ramaty, R. 1985, *ApJ*, 298, 400
 Fermi, E. 1949, *Phys. Rev.*, 75, 1169
 Fleishman, G. D., Gary, D. E., & Nita, G. M. 2003, *ApJ*, 593, 571
 Fletcher, L., & Martens, P. C. H. 1998, *ApJ*, 505, 418
 Fragos, T., Rantziou, M., & Vlahos, L. 2004, *A&A*, in press
 Heyvaerts, J. 1981, in *Solar Flare Magnetohydrodynamics*, ed. E. R. Priest (New York: Gordon), 429

- Holman, G. D. 2003, *ApJ*, 586, 606
- Holman, G. D., & Pesses, M. E. 1983, *ApJ*, 267, 837
- Holman, G. D., Sui, L., Schwartz, R. A., & Emslie, A. G. 2003, *ApJ*, 595, L97
- Hudson, H. S., & Famık, F. 2002, in Proc. 10th European Solar Physics Meeting, *Solar Variability: From Core to Outer Frontiers*, ed. A. Wilson (ESA SP-506; Noordwijk: ESA), 261
- Islaker, H., Anastasiadis, A., & Vlahos, L. 2000, *A&A*, 363, 1134
- . 2001, *A&A*, 377, 1068
- Islaker, H., Anastasiadis, A., Vassiliadis, D., & Vlahos, L. 1998, *A&A*, 335, 1085
- Islaker, H., & Vlahos, L. 2003, *Phys. Rev. E*, 67, 026413
- Kirk, J. G. 1994, *Plasma Astrophysics* (Berlin: Springer), 225
- Krucker, S., & Lin, R. P. 2002, *Sol. Phys.*, 210, 229
- Kuijpers, J. 1996, in *Plasma Astrophysics*, ed. C. Chiuderi & G. Einaudi (Heidelberg: Springer), 101
- Lee, J., Gallagher, P. T., Gary, D. E., Nita, G. M., Choe, G. S., Bong, S.-CH., & Yun, H. S. 2003, *ApJ*, 585, 524
- Lin, R. P., et al. 2002, in Proc. 10th European Solar Physics Meeting, *Solar Variability: From Core to Outer Frontiers*, ed. A. Wilson (ESA SP-506; Noordwijk: ESA), 1035
- . 2003, *ApJ*, 595, L69
- Litvinenko, Y. E. 2003, *Sol. Phys.*, 212, 379
- Lu, E. T., & Hamilton, R. J. 1991, *ApJ*, 380, L89
- Lu, E. T., Hamilton, R. J., McTiernan, J. M., & Bromund, K. R. 1993, *ApJ*, 412, 841
- Martens, P. C. H. 1988, *ApJ*, 330, L131
- Masuda, S., Kosugi, T., Hara, H., Tsuneta, S., & Ogawara, Y. 1994, *Nature*, 371, 595
- McIntosh, S. W., Charbonneau, P., Norman, J. P., Bogdan, T. J., & Liu, H. L. 2002, *Phys. Rev. E*, 65, 46125
- Melrose, D. B. 1992, in *Particle Acceleration in Cosmic Plasmas*, ed. G. P. Zank & T. K. Gaisser (New York: AIP), 3
- Miller, J. A., & Roberts, D. A. 1995, *ApJ*, 452, 912
- Miller, J. A., et al. 1997, *J. Geophys. Res.*, 102, 14631
- Moghaddam-Taaheri, E. L., & Goertz, C. K. 1990, *ApJ*, 352, 361
- Moghaddam-Taaheri, E. L., Vlahos, L., Rowland, H. L., & Papadopoulos, K. 1985, *Phys. Fluids*, 28, 3356
- Nordlund, A., & Galsgaard, K. 1996, in *Solar and Heliospheric Plasma Physics*, ed. G. M. Simnett, C. A. Allisandrakis, & L. Vlahos (Berlin: Springer)
- Parker, E. N., 1988, *ApJ*, 330, 474
- Piana, M., Massone, A. M., Kontar, E. P., Emslie, A. G., Brown, J. C., & Schwartz, R. A. 2003, *ApJ*, 595, L127
- Ramaty, R. 1969, *ApJ*, 158, 753
- Saint-Hilaire, P., & Benz, A. O. 2002, *Sol. Phys.*, 210, 287
- Shibata, K., Masuda, S., Shimojo, M., Hara, H., Ykoyama, T., Tsuneta, S., Kosugi, T., & Ogawara, Y. 1995, *ApJ*, 451, L83
- Sui, L., Holman, G. D., Dennis, B. R., Krucker, S., Schwartz, R. A., & Tolbert, K. 2002, *Sol. Phys.*, 210, 245
- Vlahos, L. 1993, in *Statistical Description of Transport in Plasmas, Astro- and Nuclear Physics*, ed. J. Misquich, G. Pelletier, & P. Schuck (New York: Nova), 235
- . 1994, *Space Sci. Rev.*, 68, 39
- . 1996, in *ASP Conf. Ser. 93, Radio Emission from the Stars and the Sun*, ed. A. R. Taylor & J. M. Paredes (San Francisco: ASP), 355
- Vlahos, L., Georgoulis, M., Kluiving, R., & Paschos, P. 1995, *A&A*, 299, 897
- Vlahos, L., et al. 1984, in *Energetic Phenomena on the Sun*, ed. M. Kundu & B. Woodgate (NASA CP-2439; Washington, DC: NASA)
- Wheatland, M. 2000, *ApJ*, 532, 1209